PREDICTION OF THE FORMING LIMIT CURVES USING GTN DAMAGE MODEL

ABDOLVAHED KAMI[1], BIJAN MOLLAEI DARIANI[1], ALI SADOUGH VANINI[1], DAN SORIN COMSA[2], DOREL BANABIC[2]

Abstract. In this paper, the forming limit curve of an AA6016-T4 sheet metal is constructed using Gurson-Tvergaard-Needleman (GTN), Marciniak-Kuczynski (M-K) and Modified Maximum Force Criterion (MMFC) models. The mechanical behavior of the matrix material is described using Hill'48 quadratic yield criterion and an isotropic hardening rule. The accuracy of the predicted forming limit curves is checked by comparison with an experimental forming limit curve. The forming limit curve obtained by the anisotropic GTN damage model is in better agreement with the experimental results especially in the biaxial tension region. While the M–K model predicts the left branch of the forming limit curve with high accuracy, it provides poor results with high overestimation along right branch of the forming limit curve. Also, the MMFC model overestimates the forming limits. These results indicate that the GTN model is a useful tool in analyzing the formability of anisotropic sheet metals.

Key words: sheet metals, GTN damage model, formability, anisotropy.

1. INTRODUCTION

In sheet metal forming it is very important to predict the possibility of necking or fracture occurrence for different loading conditions. One of the most common tools used for this purpose is the forming limit curve (FLC). This curve is actually a plot of the major principal strain vs. minor principal strain characterizing the onset of sheet necking. Consequently, FLC divides the possible combinations of the major and the minor strains into safe and unsafe regions. More precisely, the strain combinations which stand below the FLC are considered as safe (acceptable), while the strain combinations located above the FLC are considered as unsafe.

The literature survey shows that many attempts have been to determine the forming limit curve using a variety of experimental, theoretical and numerical methods. In general, the experimental determination of FLC is a very expensive

[1] Amirkabir University of Technology, Mechanical Engineering Department, 424 Hafez Ave, 15875–4413 Tehran, Iran

[2] Technical University of Cluj-Napoca, CERTETA Research Centre, Str. C. Daicoviciu nr. 15, 400020 Cluj-Napoca, Romania

Rom. J. Techn. Sci. – Appl. Mechanics, Vol. 59, N° 3, P. 253–264, Bucharest, 2014

and time consuming process. For this reason many attempts have been made to construct the FLC by theoretical and numerical methods [1–3]. One of the suitable theoretical approaches for the FLC determination is the Gurson-Tvergaard-Needleman (GTN) damage model [4–7]. The original formulation of this model has been proposed by Gurson [4] by assuming that the degradation of the load carrying capacity and finally the fracture of ductile metals are caused by the evolution of voids. Gurson's model takes into account only the growth of pre-existing voids, without assuming any generative mechanisms. In order to overcome this limitation, Tvergaard and Needleman [5–7] have proposed mathematical descriptions of the void nucleation and coalescence. The final modified model is known as Gurson-Tvergaard-Needleman (GTN) damage model.

Of course, it is possible to solely use the GTN damage model to predict the fracture of the ductile materials during deformation. On the other hand, the GTN model could be also used to construct the forming limit curve. Brunet et al. [8] studied the occurrence of necking in square cup deep drawing of a mild-steel sheet and also extracted the limit strains of the sheet using an anisotropic Gurson-Tvergaard criterion [4, 5]. Brunet et al. [9, 10] proposed a necking criterion based on the load-instability and plane strain localization assumptions in which the failure of the material is defined by an anisotropic Gurson–Tvergaard damage model. He et al. [11] predicted the forming limit stress diagram of 5052 aluminum alloy based on the GTN model. Abbasi et al. [12, 13] used GTN model to predict the forming limit curve of an IF-steel and a tailor welded blank made from IF-steel.

In this paper, a GTN model based on Hill's quadratic expression of the equivalent stress is used to construct the forming limit curve. The model is implemented as a VUMAT routine in the ABAQUS/Explicit finite-element code. Furthermore, the plastic strain and void volume fraction distributions near the fracture section are analyzed.

2. GTN DAMAGE MODEL

The GTN model [5–7] considers an isotropic plastic deformation for the matrix material. On the other hand, as the metallic sheets are produced by rolling processes, some plastic anisotropy is induced in the matrix material. For this reason, to obtain more accurate results, it is more realistic to assume a plastic anisotropy of the matrix material. So, the Hill'48 equivalent stress [14] is used to describe the plastic anisotropy.

Hill'48 equivalent stress is expressible as follows [14]:

$$\bar{\sigma} = \left[\begin{matrix} F(\sigma_{22} - \sigma_{33})^2 + G(\sigma_{33} - \sigma_{11})^2 + H(\sigma_{11} - \sigma_{22})^2 + \\ 2L\sigma_{23}^2 + 2M\sigma_{31}^2 + 2N\sigma_{12}^2 \end{matrix} \right]^{1/2}. \tag{1}$$

The quantities denoted as σ_{ij} (i, j = 1, 2, 3) in Eq. (1) are Cartesian components of a Cauchy stress tensor expressed in a frame that follows the local rotation of the anisotropy axes, while F, G, H, L, M and N are material constants. The parameters F, G, H, L, M and N can be evaluated using different types of experimental data. In the case of metallic sheets, the standard identification procedure relies on the Lankford coefficients r_0, r_{45} and r_{90} obtained from uniaxial tensile tests performed on specimens cut at 0°, 45° and 90° with respect to the rolling directions. The following relationships can be used to evaluate the parameters F, G, H, L, M and N when these coefficients are available:

$$\begin{aligned} &F = \frac{H}{r_{90}}, \quad G = \frac{H}{r_0}, \quad H = \frac{r_0}{r_0 + 1}, \\ &L = M = \frac{3}{2}, \quad N = \frac{(r_0 + r_{90})(2r_{45} + 1)}{2r_{90}(r_0 + 1)}. \end{aligned} \tag{2}$$

The general form of the GTN damage potential is:

$$\Phi = \left(\frac{\overline{\sigma}}{Y}\right)^2 + q_1 f^* \left[2\cosh\left(-q_2 \frac{3p}{2Y}\right) - \frac{q_3}{q_1} f^*\right] - 1, \tag{3}$$

where $\overline{\sigma}$ is the equivalent stress defined by Eq. (1), p is the hydrostatic pressure, Y is the yield stress of the matrix material defined as a function of the equivalent plastic strain $\overline{\varepsilon}^p$ by means of Swift's hardening law:

$$Y(\overline{\varepsilon}^p) = K(\varepsilon_0 + \overline{\varepsilon}^p)^n, \tag{4}$$

and

$$f^* = \begin{cases} f, & \text{if} \quad f \le f_C, \\ f_C + \dfrac{f_f^* - f_C}{f_f - f_C}(f - f_C), & \text{if} \quad f_C < f < f_f, \\ f_f^*, & \text{if} \quad f \ge f_f \end{cases} \tag{5}$$

is a porosity parameter depending on the current void volume fraction f The quantity f^* has been introduced by Tvergaard and Needleman [7] to describe the accelerated loss of load carrying capacity due to the coalescence of voids. All the other symbols occurring in Eqs (3), (4) and (5) are material constants. The change of the void volume fraction f is caused by the growth of the initial void volume fraction f_0 and the nucleation of new voids at the limits of the second phase particles and inclusions:

$$\dot{f} = \dot{f}_{\text{growth}} + \dot{f}_{\text{nucleation}}, \tag{6}$$

where

$$\dot{f}_{\text{growth}} = (1-f)\left[\dot{\varepsilon}_{11}^{(p)} + \dot{\varepsilon}_{22}^{(p)} + \dot{\varepsilon}_{33}^{(p)}\right] \tag{7}$$

and

$$\dot{f}_{\text{nucleation}} = \frac{f_N}{S_N\sqrt{2\pi}}\exp\left[-\frac{1}{2}\left(\frac{\bar{\varepsilon}^{(p)} - \bar{\varepsilon}_N}{S_N}\right)^2\right]. \tag{8}$$

The quantities denoted as S_N, $\bar{\varepsilon}_N$ and f_N in Eq. (8) are also material constants. The values of q_1, q_2, $q_3 = q_1^2$, S_N and $\bar{\varepsilon}_N$ have been adopted as 1.5, 1, 2.25, 0.1 and 0.3 [15], respectively. The values of the other parameters, i.e. f_0, f_C, f_F and f_N, have been obtained using an identification procedure which employs the central composite design and response surface methodology (RSM). In this way, the optimum values of f_0, f_C, f_F and f_N parameters have been calculated as 0.00035, 0.05, 0.05 and 0.15, respectively. The complete procedure followed to obtain these values is explained in detail in our previously published papers [16, 17].

3. NUMERICAL DETERMINATION FORMING LIMIT CURVE

The commercial ABAQUS/Explicit finite element code and the VUMAT implementation of the anisotropic GTN damage model have been used to calculate the forming limit curve of an AA6016-T4 sheet (1 mm thickness). The mechanical properties of this material have been determined from uniaxial tensile tests performed on specimens cut at 0°, 45° and 90° with respect to the rolling direction. The Lankford coefficients obtained from these tests are the following ones: $r_0 = 0.5529$, $r_{45} = 0.4091$ and $r_{90} = 0.5497$. The values of material constants in the Swift's law have been obtained as: $K = 525.77$ MPa, $\varepsilon_0 = 0.01125$ and $n = 0.27$. Furthermore, Young's modulus E = 70 GPa and Poison's ratio $\nu = 0.33$ have been also evaluated by averaging the results of the uniaxial tensile tests associated to the 0°, 45° and 90° directions.

To construct the numerical forming limit curve, several Nakajima tests have been simulated using the finite element code ABAQUS/Explicit and the VUMAT implementation of the GTN model. In each case, the major and minor principal surface strains at the onset of necking have been determined by processing the strain maps with the ARAMIS software. Figure 1 shows the finite element model of the Nakajima test performed on a specimen having the shaft width w = 55 mm. Because of the anisotropic behavior of the material, the specimens have been

modeled with full geometry, as shown in Fig. 1. A holding force of 100 kN has been applied to the reference point of the blank holder.

The die, punch and the blank holder have been modeled as analytical rigid surfaces, while the specimen has been meshed using hexahedral elements with 8 nodes and reduced integration (C3D8R). The frictional interactions between the metallic sheet and tools have been described using Coulomb's model. The following values of the friction coefficient have been adopted: 0.03 at the interface with the punch, and 0.1 for the interfaces with the clamping ring and die.

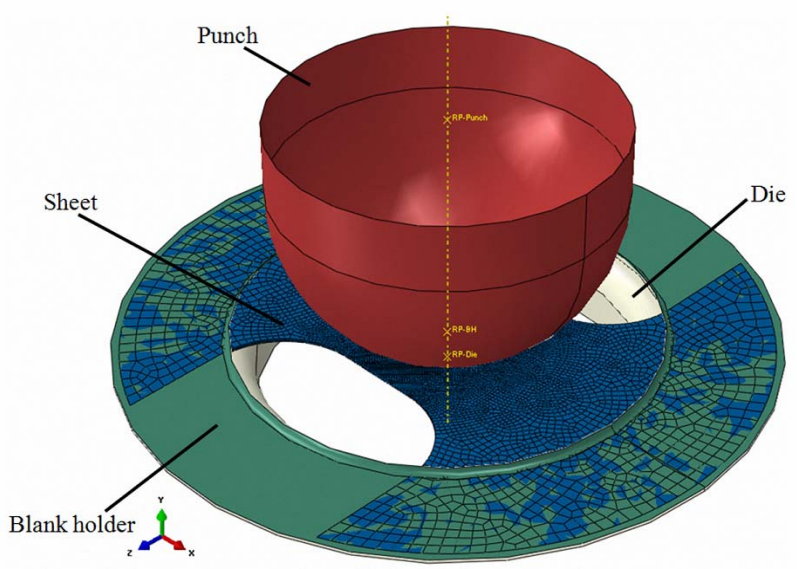

Fig. 1 – Finite element model of a Nakajima test.

4. EXPERIMENTAL DETERMINATION FORMING LIMIT CURVE

The performances of the constitutive model implemented as a VUMAT routine have been assessed by calculating the forming limit curve of an AA6016-T4 metallic sheet (1 mm thickness) and comparing the numerical predictions with reference data obtained from a series of Nakajima tests [18]. Punch stretching tests performed on specimens with different shaft widths (denoted as w in Fig. 2) allow the reproduction of different load states ranging from uniaxial traction (small values of the shaft width) to balanced-biaxial traction (case of a fully circular specimen). These loads cover both branches of a forming limit curve. The values of the width parameter w adopted by the authors are 30, 55, 70, 90, 120, 145 and 185 mm, the last of them corresponding to a fully circular specimen.

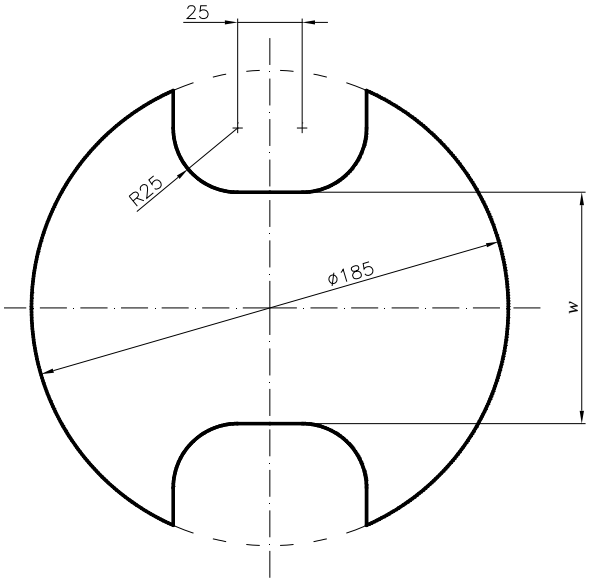

Fig. 2 – Dimensional characteristics of the specimens used in the Nakajima tests.

5. DETERMINATION OF FORMING LIMIT CURVE USING M-K AND MMFC MODELS

The Marciniak-Kuczynski (M-K) model assumes that the strain localization results from a thickness imperfection schematically represented as a groove in Fig. 3 [2,19]. According to this hypothesis, two regions of the sheet metal should be distinguished: *A* – non-defective zone; *B* – groove. At different stages of the straining process, the parameter $f = s^{(B)}/s^{(A)}$, $0 < f < 1$, is used to describe the amplitude of the imperfection ($s^{(A)}$ and $s^{(B)}$ denote the current thickness of regions *A* and *B*, respectively – see Fig. 3). The mechanical interconnection $A-B$ is defined by a set of relationships enforcing the continuity of the strain-rate along the groove and the equilibrium of the normal and tangential loads acting on the interface from both sides [18]. In the case of the M-K model, necking is a consequence of the fact that the thickness strain tends to accumulate faster in region *B*.

The Modified Maximum Force Criterion (MMFC) proposed by Hora et al. [20] is an extension of Considère's model. The basic idea behind the MMFC model is the assumption that necking is preceded by a local evolution of the material towards the plane strain state (Fig. 4). Using this hypothesis, Hora and his co-workers were able to define an analytical relationship from which the limit strains corresponding to different load paths could be determined [18].

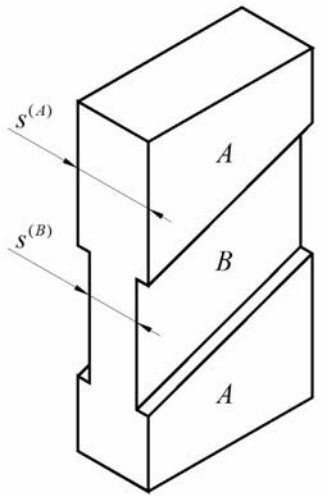

Fig. 3 – Schematic view of the thickness imperfection assumed by the M-K model.

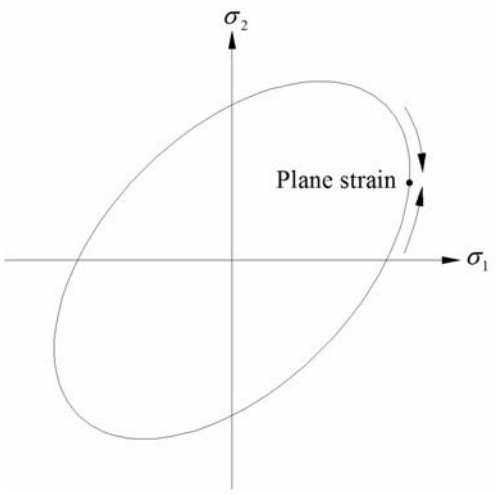

Fig. 4 – Evolution towards the plane strain point of a yield locus assumed by the MMFC model.

6. RESULTS AND DISCUSSIONS

It is possible to obtain useful information about the deformation of the specimens by following the evolution of voids. This technique is able to catch the onset of necking, which is required for the construction of the forming limit curve. The distribution of the voids in the specimen with $w = 130$ mm at the start of the void coalescence process is shown in Fig. 5a. One may easily notice that the void

distribution is almost uniform in the polar region of the specimen. Figure 5b shows the voids distribution at the onset of necking. One may notice that the high values of void volume fraction are concentrated in a small region of the specimen (necking zone) while the other regions are characterized by smaller values of the void volume fraction and almost uniform distributions of this quantity.

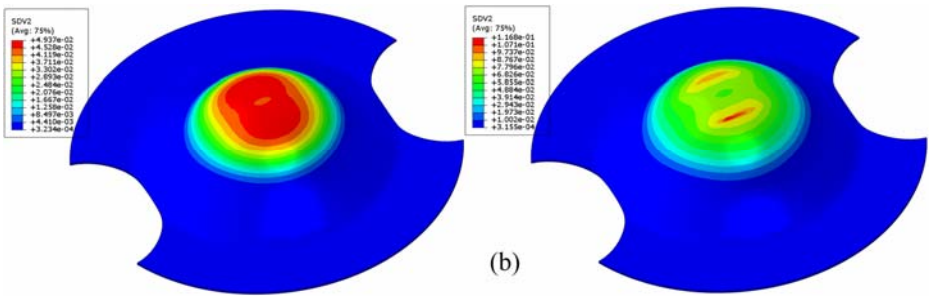

Fig. 5 – Void volume distribution on the notched specimen with w = 130 mm:
a) before coalescence; b) at the onset of necking.

Figure 6 shows the distribution of the major logarithmic strain on the surface of the fractured specimen determined by numerical simulation of the punch stretching experiment performed on a notched specimen having the initial shaft width $w = 130$ mm . As shown in Fig. 6, the fracture does not occur at the dome apex (see also Fig. 5 for the case of necking). This phenomenon is the effect of the frictional contact between the punch and the specimen which limits the straining of the sheet regions in contact with the punch. Figure 6b shows a specimen fractured during the laboratory tests. The shape of the fracture region obtained by numerical simulation (Fig. 6a) compares well with the experimental results. The fractured dome height predicted by the numerical simulation (38.47 mm) is also in very good agreement with the experimental data (38 mm).

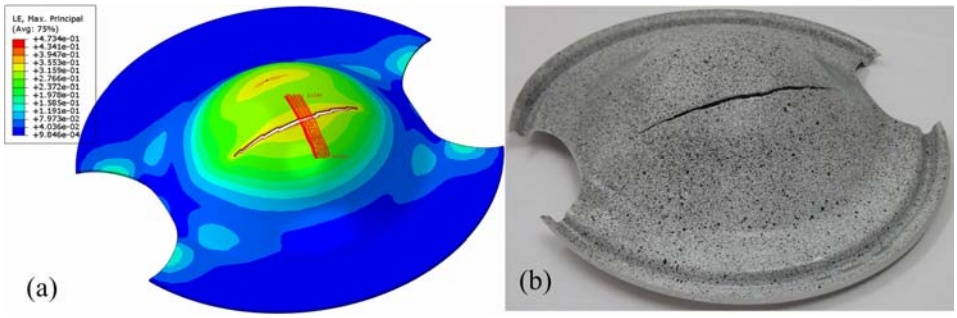

Fig. 6 – Void volume distribution on the notched specimen with w = 130 mm at fracture:
a) finite element simulation; b) image of the specimen used in the experimental test.

The forming limit curve obtained using the ARAMIS software is presented in Fig. 7, which indicates that the results obtained by numerical simulation using the GTN damage model are in good agreement with the experimental data. The comparison becomes even more favorable when confronted with the predictions of the Marciniak-Kuczynski (M-K) model and the Modified Maximum Force Criterion (MMFC) – see Fig. 7. One may notice from the diagram that the quality of the GTN predictions is far better, especially along the right branch of the forming limit curve, where both M-K and MMFC models overestimate the formability of the metallic sheet. The overestimation is totally unrealistic along the right branch of the forming limit curve. The idealizations included in the M-K and MMFC models seem to be responsible for the poor quality of the numerical predictions. In contrast, the finite-element analysis based on the GTN constitutive model is able to describe the actual conditions of a Nakajima test with better accuracy. The authors consider this fact as the main explanation for the quality of the finite-element results.

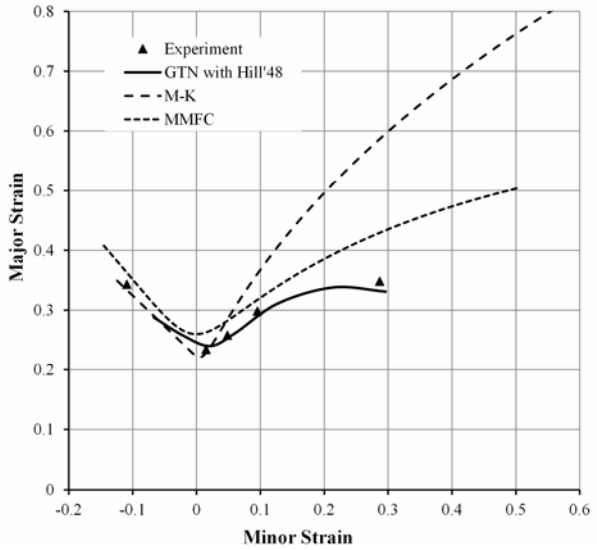

Fig. 7 – Comparison between the FLCs obtained by different methods.

The strain distribution corresponding to the fracture moment has been also used for the determination of the forming limit curve by means of Bragard's method. Figure 8 shows the values of the strains at the necking and fracture moment at the middle of a crack region (see Fig. 6a). By comparing the values of strains at the fracture moment, one may notice that the strain values are not far from those obtained by processing the frame associated to the necking stage of the specimen. This is a consequence of the fact that after necking the strains evolve only in a small region of the specimen. The limit strains calculated by the ARAMIS

software are almost the same for both necking and fracture stages (with negligible differences). This is the consequence of the exclusion of the middle points from the major and minor strain calculations. In this way, the forming limit curve constructed using the fracture frame (Fig. 9) is very similar to the forming limit curve obtained by processing the necking frame. In some cases, because of the elastic relaxation after the fracture, the limit strains obtained from the fracture frame are somewhat lower than those determined on the basis of the necking frame (see the right branch of the forming limit curve shown in Fig. 9).

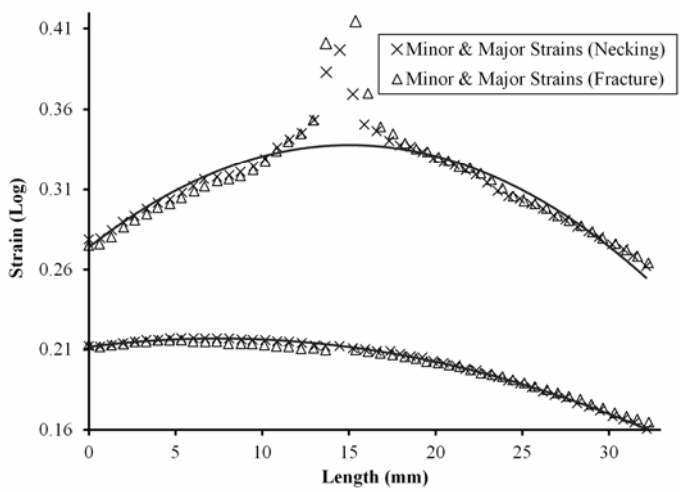

Fig. 8 – Determination of the major and minor in the notched specimen with w = 130 mm.

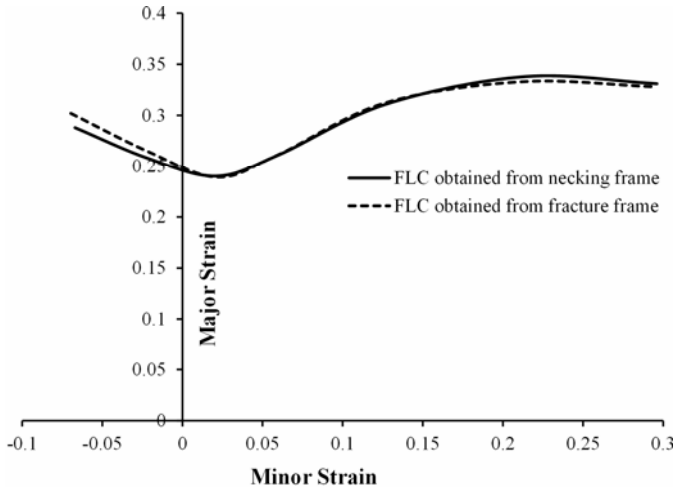

Fig. 9 – Comparison between the forming limit curves obtained at the onset of necking and after the fracture.

7. CONCLUSIONS

In this research, the anisotropic GTN damage model with Hill'48 quadratic yield criterion, M-K and MMFC models were used to construct the forming limit curve of a metallic sheet. The forming limit curve of the AA6016-T4 aluminum alloy was computed by simulating a sequence of Nakajima tests with the finite element code ABAQUS/Explicit and a VUMAT implementation of the GTN damage model. The numerical forming limit curve showed a good agreement with the experimental results. In general, the limit strains predicted by the GTN model were more accurate than those calculated with the M-K and MMFC models. The numerical forming limit curve of the AA6016-T4 aluminum alloy was also determined by processing the distribution of the principal strains associated to the fracture stage of the Nakajima test. The results showed that this curve is almost coincident with the forming limit curve obtained using the onset of necking. The analysis of the plastic strain and void volume fraction distributions showed that they are useful tools for detecting the onset of necking and the final fracture. In the numerical determination of the forming limit diagrams, these distributions can be used to make the decision about the moment and location of the limit strain measurement.

Received on November 7, 2014

REFERENCES

1. HILL, R., *On discontinuous plastic states, with special reference to localized necking in thin sheets*, J. Mech. Phys. Solids, **1**, *1*, pp. 19–30, 1952.
2. MARCINIAK, Z., KUCZYNSKI, K., *Limit strains in processes of stretch-forming sheet metal*, Int. J. Mech. Sci., **9**, *9*, pp. 609–620, 1967.
3. LI, B., NYE, T.J., WU, P.D., *Predicting the forming limit diagram of AA 5182-O*, J. Strain Anal. Eng., **45**, *4*, pp. 255–273, 2010.
4. GURSON, A.L., *Continuum theory of ductile rupture by void nucleation and growth Part I-Yield criteria and flow rules for porous ductile media*, J. Eng. Mater. Tech., **99**, *1*, pp. 2–15, 1977.
5. TVERGAARD, V., *Influence of voids on shear band instabilities under plane strain conditions*, Int. J. Fract., **17**, *4*, pp. 389–407, 1981.
6. TVERGAARD, V., *On localization in ductile materials containing spherical voids*, Int. J. Fract., **18**, *4*, pp. 237–252, 1982.
7. TVERGAARD, V., NEEDLEMAN, A., *Analysis of the cup-cone fracture in a round tensile bar*, Acta Metallurgica, **32**, *1*, pp. 157–169, 1984.
8. BRUNET, M., MORESTIN, F., MGUIL, S., *The Prediction of Necking and Failure in 3 D. Sheet Forming Analysis Using Damage Variable, Analytical and experimental studies of necking in sheet metal forming processes*, J. Phys. IV (France), **06**, *C6*, pp. C6-473-C6-482, 1996.
9. BRUNET, M., MGUIL, S., MORESTIN, F., *Analytical and experimental studies of necking in sheet metal forming processes*, J. Mater. Proc. Tech., **80–81**, *1*, pp. 40–46, 1998.

10. BRUNET, M., MORESTIN, F., *Experimental and analytical necking studies of anisotropic sheet metals*, J. Mater. Proc. Tech., **112**, *2–3*, pp. 214–226, 2001.
11. HE, M., LI, F., WANG, Z., *Forming Limit Stress Diagram Prediction of Aluminum Alloy 5052 Based on GTN Model Parameters Determined by In Situ Tensile Test*, Chin. J. Aeronaut., **24**, *3*, pp. 378–386, 2011.
12. ABBASI, M., SHAFAAT, M.A., KETABCHI, M., HAGHSHENAS, D.F., ABBASI, M., *Application of the GTN model to predict the forming limit diagram of IF-Steel*, J. Mater. Proc. Tech., **26**, *2*, pp. 345–352, 2012.
13. ABBASI, M., BAGHERI, B., KETABCHI, M., HAGHSHENAS, D.F., *Application of response surface methodology to drive GTN model parameters and determine the FLD of tailor welded blank*, Comput. Mater. Sci., **53**, *1*, pp. 368–376, 2012.
14. HILL, R., *A theory of the yielding and plastic flow of anisotropic metals*, Roy. Soc. London Proc. A., **193**, *1033*, pp. 281–297, 1948.
15. BENSEDDIQ, N., IMAD, A., *A ductile fracture analysis using a local damage model*, Int. J. Pres. Ves. Pip., **85**, *4*, pp. 219–227, 2008.
16. KAMI, A., MOLLAEI DARIANI, B., SADOUGH VANINI, A., COMSA, D. S., BANABIC, D., *Application of a GTN damage model to predict the fracture of metallic sheets subjected to deep-drawing*, Proc. Rom. Acad. Series A., **15**, *3*, pp. 300–309, 2014.
17. KAMI, A., MOLLAEI DARIANI, B., SADOUGH VANINI, A., COMSA, D. S., BANABIC, D., *Numerical determination of the forming limit curves of anisotropic sheet metals using GTN damage model*, J. Mater. Proc. Tech., **216**, pp. 472–483, 2015.
18. BANABIC, D., *Formability of Sheet Metals* (Chap. 3), in *Sheet Metal Forming Processes*, D. Banabic (Ed.), Springer, Heidelberg, 2010, pp. 141–211.
19. HUTCHINSON, R. W., NEALE, K. W., *Sheet necking I*, in *Mechanics of Sheet Metal Forming*, D. P. Koistinen, N. M. Wang (Eds.), Plenum Press, New York/London, 1978, pp. 111–126.
20. HORA, P., TONG, L., *Prediction methods for ductile sheet metal failure using FE-simulation*, Proceedings of the 18th Biennial IDDRG Congress, May 16–17, 1994, Lisbon, pp. 363–375.